AGU PUBLICATIONS

JGR

Journal of Geophysical Research: Space Physics

RESEARCH ARTICLE
10.1002/2016JA023647

Key Points:
- First observation of *F* region bottom-type irregularity scattering layer (BSL) generated before sunset
- Similar oscillations found in BSL echo Doppler velocity and *F* layer height
- The presunset BSL could be linked with the presunset *F* region bottomside large-scale wave structure

Correspondence to:
G. Li,
gzlee@mail.iggcas.ac.cn

Citation:
Li, G., B. Ning, M. A. Abdu, W. Wan, C. Wang, G. Yang, K. Liu, L. Liu, and C. Yan (2017), First observation of presunset ionospheric *F* region bottom-type scattering layer, *J. Geophys. Res. Space Physics*, *122*, 3788–3797, doi:10.1002/2016JA023647.

Received 2 NOV 2016
Accepted 13 MAR 2017
Accepted article online 15 MAR 2017
Published online 27 MAR 2017

First observation of presunset ionospheric *F* region bottom-type scattering layer

Guozhu Li[1,2], Baiqi Ning[1,2], M. A. Abdu[3,4], Weixing Wan[1,5], Chi Wang[2,6], Guotao Yang[2,6], Kangkang Liu[1], Libo Liu[1,5], and Chunxiao Yan[2,6]

[1]Key Laboratory of Earth and Planetary Physics, Institute of Geology and Geophysics, Chinese Academy of Sciences, Beijing, China, [2]State Key Laboratory of Space Weather, National Space Science Center, Chinese Academy of Sciences, Beijing, China, [3]Instituto Nacional de Pesquisas Espaciais, Sao Jose dos Campos, Brazil, [4]Instituto Tecnologioc de Aeronautica, Sao Jose dos Campos, Brazil, [5]Beijing National Observatory of Space Environment, Institute of Geology and Geophysics, Chinese Academy of Sciences, Beijing, China, [6]Hainan National Observatory of Space Weather, National Space Science Center, Chinese Academy of Sciences, Beijing, China

Abstract The bottom-type irregularity scattering layer (BSL) that can appear in the ionospheric *F* region bottomside has been observed generally after sunset, serving as a possible telltale of equatorial spread *F* (ESF). Using simultaneous multibeam radar measurements over two low-latitude stations, Sanya (18.3°N, 109.6°E; dip latitude 13°N) and Fuke (19.3°N, 109.1°E; dip latitude 14°N) in China, we report, for the first time, a thin BSL that initially occurred at presunset (~1720 LT), much earlier than the occurrence of BSL generated from the equatorial plasma shear vortex-driven instability. The presunset BSL was situated around 225 km altitude and continued to exist until the appearance of ESF plumes after sunset (~1930 LT). Interestingly, the Doppler velocities of the presunset BSL echoes measured by the radar and the *F* layer virtual heights obtained from the collocated Digisonde measurements over Sanya both show oscillations with a period of about 1 h, suggesting a close link between the occurrences of the BSL and of *F* region plasma density large-scale wave structure before sunset. These observations could imply an important role of gravity waves in the generation of the presunset *F* region bottom-type irregularities.

1. Introduction

Ionospheric *F* region bottom-type irregularities, which are observed as a backscattering layer with thickness typically less than 50 km in radar range-time-intensity (RTI) plots, were first discovered by *Woodman and La Hoz* [1976] with the Jicamarca radar located at the magnetic equator in Peru. This bottom-type scattering layer (BSL), named as bottom-type spread *F* by *Woodman and La Hoz*, was observed after sunset and followed by equatorial spread *F* (ESF) plume irregularities capable of producing strong ionospheric scintillations and affecting satellite communication and navigation systems. Since then, the occurrence of *F* region BSL, its generation mechanism and its possible role as a precursor to ESF plume have become important topics in the investigation of equatorial ionosphere [e.g., *Hysell and Burcham*, 1998; *Kudeki and Bhattacharyya*, 1999; *Hysell et al*., 2005; *Takahashi et al*., 2010].

After the first report on its observation over Jicamarca, the BSL has been observed at postsunset hours with other radars located near the magnetic equator, such as Pohnpei (7°N, 158.2°E; dip latitude 0.4°N) and Sao Luis (2.5°S, 44.3°W; dip latitude 1.7°S) [*Rodrigues et al*., 2004; *Tsunoda and Ecklund*, 2007a], and also at low latitudes, such as Kwajalein (8.8°N, 167.5°E; dip latitude 4°N) and Gadanki (13.5°N, 79.2°E; dip latitude 6.5°N) [*Hysell et al*., 2005; *Patra et al*., 2014]. By using the Jicamarca radar observations, *Hysell and Burcham* [1998] presented a statistical study of different types of spread *F* at equatorial latitudes, showing that the BSL frequently occurred after sunset and its occurrence probability was comparable to that of ESF plumes. These postsunset BSLs have been explained on the basis of the horizontal wind-driven interchange instability associated with the plasma shear flow at *F* region bottomside where a large differential neutral-plasma zonal velocity exists, being part of the postsunset plasma flow vortex [e.g., *Kudeki and Bhattacharyya*, 1999; *Hysell et al*., 2005]. At low latitudes, results from the Gadanki VHF radar showed that *F* region BSL occasionally occurred preceding ESF development [*Patra et al*., 2014]. It has been suggested that the low-latitude BSL could be related to the equatorial *F* region bottomside instability process producing equatorial BSL, which appear within 200–400 km altitudes over magnetic equator and can affect low latitude through magnetic field line mapping.

The *F* region bottom-type irregularities, though appearing as a continuous echoing layer in radar RTI plot, are not necessarily distributed uniformly in space but could be clustered into patches in the east-west direction with a periodicity similar to that of the *F* region density wave structure and/or periodic ESF plumes [*Hysell et al*., 2005]. Based on the measurements by a VHF coherent radar, two ionosondes and two all-sky airglow imagers in Brazil, *Takahashi et al*. [2010] reported a case where BSL and *F* region density large-scale wave structures (LSWS) extending more than 1500 km in the longitudinal direction were simultaneously observed. These observations showed a good correlation between the occurrences of LSWS and of BSL during postsunset. On the other hand, LSWS have been observed starting at both presunset and postsunset hours (around 16–20 LT) as evidenced from measurements of longitudinal variation in TEC and of temporal variation in *F* layer heights [e.g., *Abdu et al*., 2009; *Tsunoda et al*., 2010]. In this context we note, however, that no presunset *F* region BSLs have been reported yet. All cases so far reported have been concerned with BSL existing exclusively in the plasma shear flow vortex structure after sunset.

In this paper we present, to our knowledge, the first results of *F* region BSL observed before sunset. Simultaneous radar observations over Sanya (18.3°N, 109.6°E; dip latitude 13.1°N) and Fuke (19.3°N, 109.1°E; dip latitude 14.3°N) recorded a thin irregularity backscattering layer in the *F* region bottomside starting at presunset hours and continuing until the appearance of ESF plume. Although the postsunset BSL is usually thought to be generated through the equatorial plasma shear vortex-driven instability, the present BSL observed during 1720–1930 LT at low latitudes far away from the magnetic equator, however, is hard to be explained by the equatorial mechanism. Possible factors responsible for the occurrence of the presunset BSL are discussed.

2. Observational Setup

The Sanya and Fuke VHF radars, with operating frequencies of 47.5 MHz and 47 MHz and peak powers of 24 kW and 54 kW, respectively, have been employed to investigate ionospheric 3 m scale irregularities over Hainan Is., China [e.g., *Li et al*., 2012, 2016; *Chen et al*., 2015]. The Sanya radar antenna array is composed of six modules (each includes 2×2 Yagi antennas) aligned in the east-west direction for transmission and reception, and one additional module installed in the north of the east-west array for reception. The Fuke radar was built in 2010 under the support of the Chinese meridian project [e.g., *Wang*, 2010]. Its antenna array is composed of 4×18 Yagi antennas. Both radars have a capability to steer the beam in the east-west direction. In this study, the Sanya and Fuke radar beams were steered in five and seven directions, with temporal (range) resolutions of about 5 and 2 min (2.55 and 0.711 km), respectively. For Sanya (Fuke) radar, the pulse repetition frequency was 160 Hz (200 Hz) with a 4 bit complementary (13 bit Barker) code. Note that due to the relatively wide 3 dB (half power full beam) widths of both radars (36° and 21° in the north-south direction for Sanya and Fuke radars, respectively), the perpendicularity between the radar line of sight and the magnetic field line required for detecting the ionosphere *E* and *F* region irregularity echoes can be met for all the radar beams.

Figure 1 shows the radar geographic locations, the radar beam directions (with beam number and the corresponding azimuth angle), and the altitude lines (dashed lines where the perpendicularity is met) marked at 100–400 km. The shaded area of each direction represents the region covered approximately by the 3 dB beam width. At an altitude of 200 km, the Sanya and Fuke radar scans cover about 260 km and 140 km in the east-west direction, respectively. The ionogram measurements by the collocated Digisonde Portable Sounder (DPS-4d) over Sanya with a temporal resolution of 7.5 min are used to estimate the variation of *F* layer virtual heights at plasma frequencies from 4 to 10 MHz.

3. Cases of Presunset BSL by the Sanya and Fuke Radars

Figure 2 shows a case of presunset BSL simultaneously detected by the Sanya and Fuke radars on 30 September 2015 (a geomagnetic quiet day with maximum $Kp = 1$ and minimum $Dst = 0$). The RTI plots of backscatter echoes obtained from three selected beams of the Sanya and Fuke radars are shown in Figures 2a–2c and 2d–2f, respectively. The vertical axis and the slant dashed line superimposed in Figures 2b and 2e show the height scale in altitude where the radar beam is perpendicular to the magnetic field and the sunset terminator, respectively. Local ground sunset occurred at 1748 LT on that day and the *E* region (*F* region) sunset about 44 min (70 min) later. As shown in Figure 2b (also more clearly in Figure 3a), a thin echoing layer appeared first at/before 1720 LT and continued to be present until postsunset around 1930 LT,

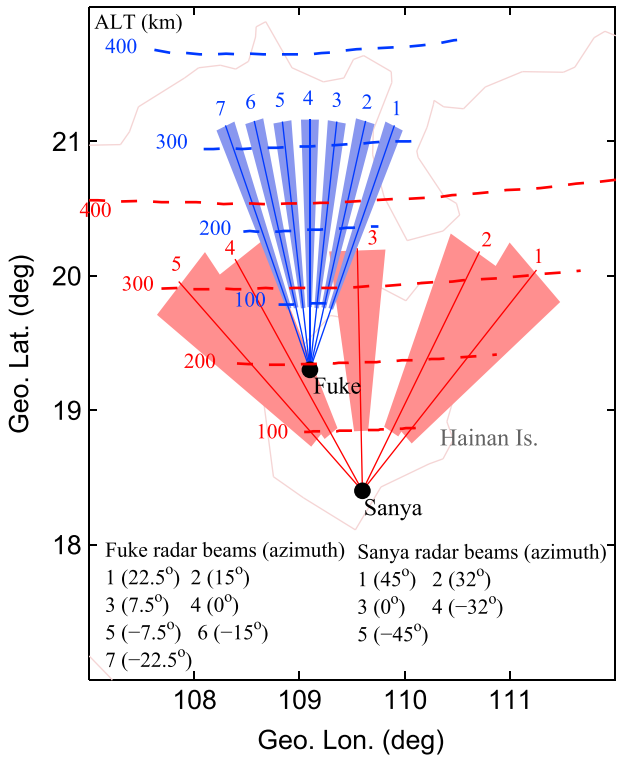

Figure 1. The Sanya and Fuke VHF radar beam directions projected on the geographic longitude-latitude plane. The shaded area in each direction represents the 3 dB (half power full beam) width.

which was followed by four ESF backscatter plumes labeled A, B, C, and D. The feature of the thin layer preceding ESF plumes resembles closely with that of the postsunset BSL observed around the magnetic equator. The thin echoing layer, with a thickness of about 10 km, situated around 225 km altitude at the *F* layer bottomside is the so-called bottom-type scattering layer. The BSL altitude shows a weak perturbation. Similar to the Sanya radar observations, the Fuke radar measurements (Figure 2e) also show that the BSL was observed well before sunset, starting from 1750 LT and lasting till 1910 LT. During the presence of the BSL, the digisonde and GPS scintillation receiver collocated at Sanya did not record any corresponding ionogram diffuse echo and ionospheric scintillation, respectively (figure not shown here), similar to what was verified in previous studies of BSL generated after sunset when no accompanying ionospheric scintillation was observed.

Another feature of interest shown in Figure 2 is that the BSL was observed only by one beam (beam 3 for both radars). The zonal distance (at an altitude of 200 km) between the illuminated volumes of the Fuke radar beams 2 and 4 (where no BSL detected) is about 30 km. This indicates that the zonal extension of the BSL echoing region was less than 30 km. The ESF plumes, however, covered a wide longitude region accompanying their eastward drifts inferred from the radar scans. The plume A was observed by all the five beams of Sanya radar, but only by the Fuke radar beams 1–4. One may note from Figure 1 that the scanned longitudes by the Sanya radar five beams were larger than that of the Fuke radar. Based on the slight difference of latitudes where the two radars located, the absence of plume A in the Fuke radar beams 5–7 could be associated with the apex altitude of the plume over magnetic equator [e.g., *Li et al*., 2016]. The plume rising to apex altitudes of 600–670 km can be detected by the Sanya radar but may not be detected by the Fuke radar. Further, the occurrence time of plume A in the RTI plots of Sanya radar beams 4–5 are nearly the same. These observations indicate that the plume A was initially generated near the longitude of Sanya radar beams 4–5 scan, not far from the longitude where the BSL was observed. As for the ESF plumes B, C, and D, which first appeared in the westernmost beam more than 2 h later after sunset, and traversed from west to east across the radar scanned area, they were generated in the western longitudes away from the radar sites [e.g., *Li et al*., 2013].

By using a similar method as that used in *Li et al*. [2012], we estimated the horizontal distances between the periodic ESF plumes A–D, which were about 500, 350, and 450 km. Based on the Kwajalein Altair radar scanning and the Jicamarca radar imaging observations, *Hysell et al*. [2005, 2006] reported that during the days with ESF plume, the bottom-type irregularities generated after sunset were usually clustered into periodic patches in the east-west direction, which were separated by a distance similar to the wavelength of LSWS and/or the horizontal separation of periodic ESF plumes. They suggested that the BSL and LSWS are modulated by the same source that seeded the ESF plumes. In the present study, if the bottom-type irregularities and periodic ESF plumes were seeded by same energy source, the BSL echoes shown in Figure 2 would be from one of the periodic bottom-type irregularity patches which could have the same periodicity as the ESF plumes (350–500 km).

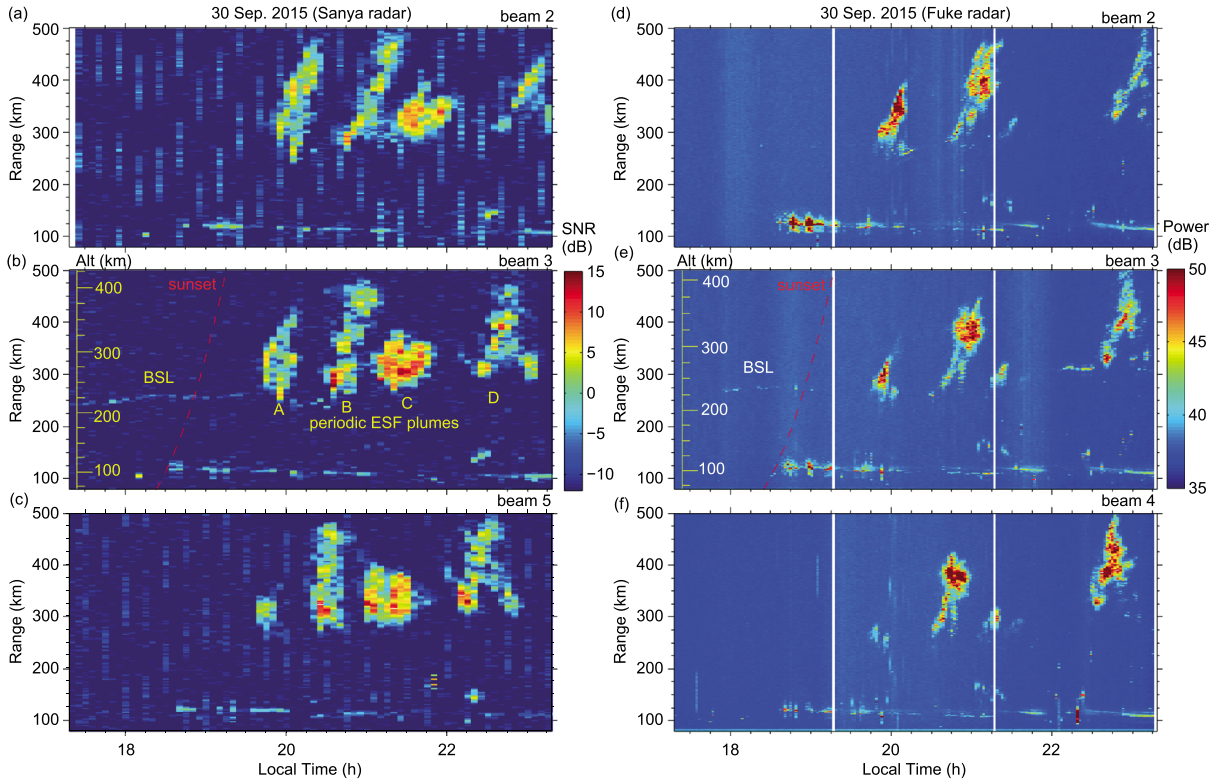

Figure 2. Range-time-intensity (RTI) maps of backscatter echoes obtained from (a–c) the Sanya and (d–f) Fuke VHF radars during 1720–2320 LT on 30 September 2015. It is evident from Figures 2b and 2e that a bottom-type irregularity echoing layer preceding periodic equatorial spread *F* (ESF) plumes (marked with A–D) was observed by the beam 3 of both radars.

Figures 3a and 3b show the Doppler spectral width (square root of second moment) and Doppler velocity of the BSL echoes shown in Figure 2b, as a function of range and time. The shaded area represents no *F* region observations during 1600–1720 LT on that day. Positive velocity indicates irregularity motion upward/northward away from the radar. The spectral widths of BSL echoes are about 10 ms^{-1}, significantly less than that of *E* region irregularity echoes and ESF plume topside echoes. The extremely narrow spectral width is similar to that of postsunset BSL reported previously [e.g., *Woodman and La Hoz*, 1976]. The velocities corresponding to the BSL echoes are always positive, indicating the presence of eastward electric fields. For the ESF plume preceded by the BSL, the Doppler velocities, in general, show positive and negative values at higher and lower altitudes, respectively. To make the temporal variation of BSL echo Doppler velocities clearer, we present in Figure 3c only the BSL echo Doppler velocities as a function of time. As indicated by the solid curve, the amplitude of Doppler velocities, in general, oscillates approximately between 12 and 17 m s^{-1} with a period of about 1 h. In this regard, we may recall from Figure 2 that the BSL altitude showed a weak oscillation. Further, we present in Figure 3d the temporal variation of *F* layer virtual heights (*h′F*, the heights of *F* layer trace in ionograms) at seven fixed plasma frequencies from 4 to 10 MHz over Sanya. The height of BSL is also included in the plot. It can be noted that during the period from 1640 to 1840 LT, the *F* layer virtual heights showed two small-amplitude oscillations with a period of about 1 h. The oscillation phase seems to propagate downward (as represented by slant solid lines), indicating upward propagation of large-scale gravity waves.

4. Preliminary Statistics of the Presunset BSL

Given that the presunset large-scale wave structure seems not rare [e.g., *Tsunoda et al.*, 2010; *Abdu et al.*, 2015], an important aspect concerning its behavior is its occurrence frequency. In this regard, future efforts will be made to explore the detailed statistical behavior of presunset BSL by conducting more joint observations with the Sanya and Fuke radars. To get a preliminary statistical result, we analyzed the Sanya radar and ionosonde measurements during September–October 2015 when the radar was operated in *F* region mode (starting from presunset hours around 1720 LT). We found that presunset BSL events appeared mainly on the

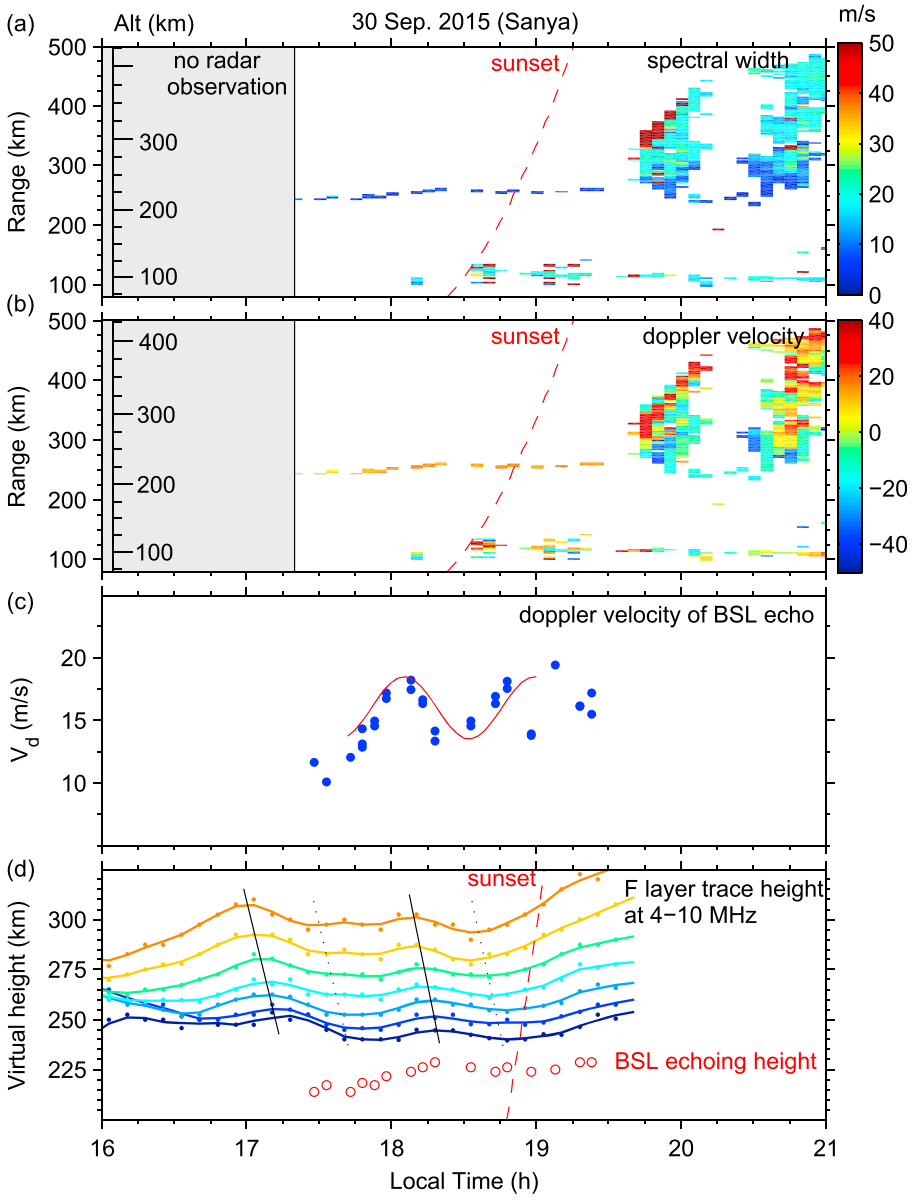

Figure 3. Range-time (a) Doppler spectral width and (b) Doppler velocity plots of irregularity echoes observed by the Sanya radar beam 3 (corresponding to Figure 2b) during 1720–2100 LT on 30 September 2015. The shaded area (gray) in the left of each panel indicates no *F* region observation. (c) Doppler velocities of BSL echoes. (d) *F* layer virtual heights (at seven plasma frequencies from 4 to 10 MHz) obtained from the Sanya ionograms. Small-amplitude oscillations can be seen in BSL echo Doppler velocity and *F* layer virtual heights.

days when presunset *F* layer height oscillations were observed. The presunset BSL events can be categorized into three types, (1) presunset BSL with *F* layer height oscillation and subsequent ESF, (2) presunset BSL with *F* layer height oscillation but without ESF, and (3) presunset BSL without obvious *F* layer height oscillation and ESF. The event shown in Figure 2 belongs to the type 1. Here we present three more presunset BSL events observed by the Sanya radar on 11 October (maximum $Kp = 4^-$ and minimum $Dst = -46$), 7 October (maximum $Kp = 7+$ and minimum $Dst = -124$), and 15 September 2015 (maximum $Kp = 4$ and minimum $Dst = -31$), respectively, in Figure 4.

As can be seen from Figure 4 (left column), BSL echoes initially appeared at presunset and continued until the presence of ESF plume with interruption around 1900 LT (observations from beam 3). Similar to that shown in Figure 3d, a small-amplitude oscillation of *F* layer virtual heights is seen around 1700–1800 LT. Figure 4

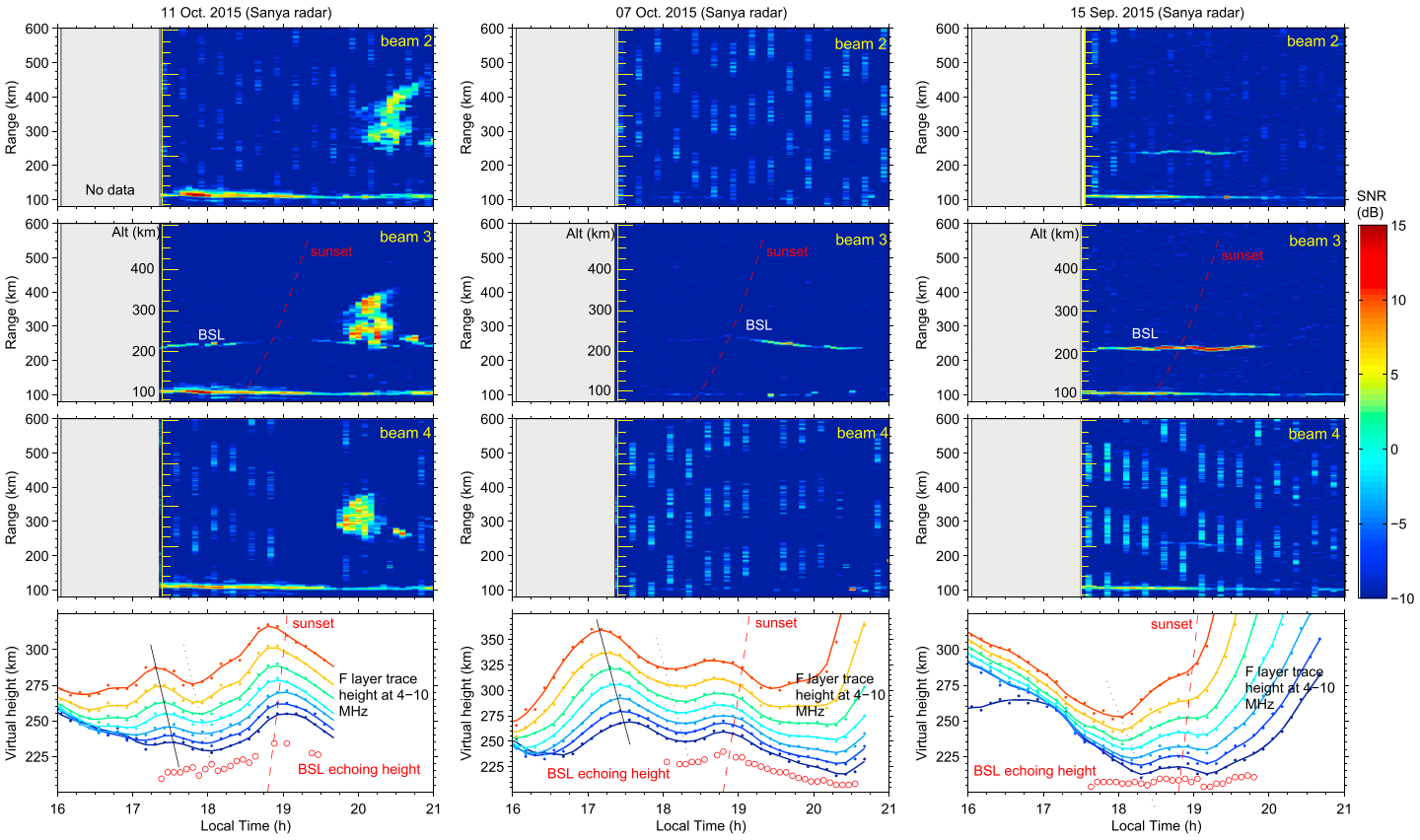

Figure 4. Three cases of presunset BSL observed by the Sanya radar on (left column) 11 October, (middle column) 7 October, and (right column) 15 September, 2015, respectively. Note that on 7 October the BSL echo intensity around 1800–1900 LT is very weak. The shaded area (gray) in the left of each RTI map indicates no *F* region observation. The bottom plots show *F* layer virtual heights at seven plasma frequencies from 4 to 10 MHz, with an interval of 1 MHz. The BSL echoing heights (shown as circles) are superimposed in the panels.

(middle column) shows the case of presunset BSL without subsequent ESF. Please note that the BSL echo intensity is very weak around 1800–1900 LT (about −5 dB), after which the echo can be clearly seen continuing until ~2040 LT, with signal-to-noise ratio (SNR) around 0–5 dB. Clear oscillations of *F* layer heights are seen around 1700–1900 LT. We note that for both the cases, the bottom-type irregularity echoes were detected only in one beam. This, however, does not necessarily indicate that the bottom-type irregularities were confined in a narrow longitudinal region. It is possible that bottom-type irregularities occurred continuously in a wide longitude region, but the backscattered signals were not strong enough to be detected at other beam directions. For example, *Tsunoda and Ecklund* [2007b] reported that if field-aligned irregularities were confined in a thin layer with sheet-like structures, the backscatter echoes would be sensitive to radar viewing directions. It may be reasonably anticipated that for horizontal thin irregularity scattering layer, maximum echo intensity would appear possibly in the vertical direction compared to beams pointing east and west. Considering that the bottom-type irregularity echoes received by the beam 3 were very weak, it is very likely that the backscattered signals from other directions were below the detection threshold of the radar.

Figure 4 (right column) shows the case of presunset BSL without obvious *F* layer altitude oscillation and ESF. The echo intensity from the vertical beam (beam 3) is apparently stronger than those of the other cases. Also, the echo intensity from this beam (beam 3) is at least 5 dB greater than those from the east and west beams. This supports the above assertion about the beam dependent appearance of BSL echoes. For this case, the *F* layer altitudes did not show obvious oscillations during/before the presence of the BSL, but a phase change can be clearly seen in the virtual heights at different plasma frequencies around 1820 LT (as represented by dotted line).

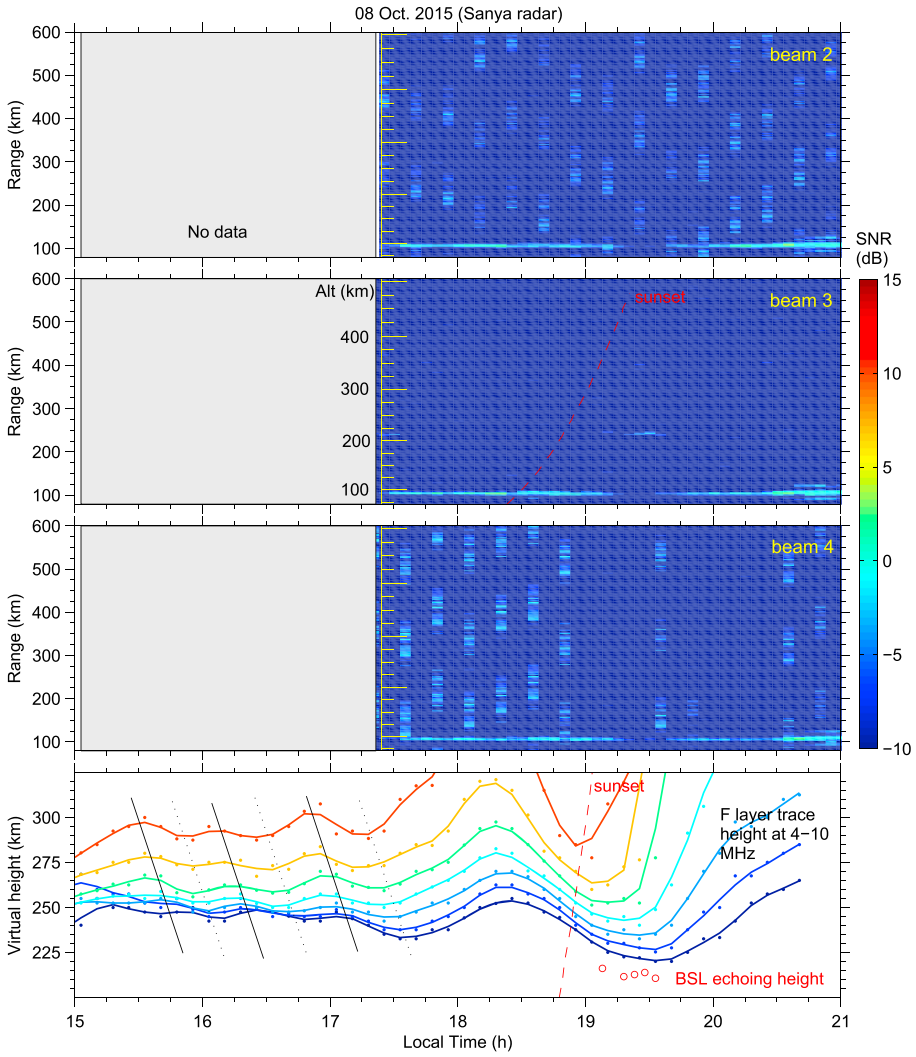

Figure 5. Sanya radar observations on 8 October 2015 (a geomagnetic disturbed day) when no obvious presunset BSL echoes detected. The fourth panel shows obvious *F* layer height oscillations observed for a long time, around 1530–1800 LT.

The events shown in Figure 4 were observed during geomagnetic disturbed days. This, however, does not necessarily represent that there is a close correlation between geomagnetic activity and BSL generation. Figure 5 shows another case observed on 8 October 2015 (maximum $Kp = 6^{-}$ and minimum $Dst = -90$). It is seen from Figure 5 (fourth panel) that obvious *F* layer altitude oscillations were observed for a long time, around 1530–1800 LT. The BSL echoes, however, were only observed during short time intervals after sunset with very weak SNR. For the present data set, we did not find a general feature on the geomagnetic activity dependency of presunset BSL. We will not make further discussion on the effect of geomagnetic activity here but only focus on the generation of presunset BSL when the *F* layer height oscillation with downward phase propagation was observed.

5. Possible Mechanisms Responsible for the Generation of Presunset BSL

The observations by the Sanya and Fuke VHF radars clearly show, for the first time, that the *F* region BSL can occur well before sunset. The altitude morphology and the extremely narrow spectral width of the presunset BSL are similar to those of postsunset BSL reported previously. In an attempt to explain the generation of presunset BSL, we may consider the mechanism known to operate in the BSL generation after sunset. With incoherent and coherent scatter radar measurements conducted at Jicamarca, *Kudeki and Bhattacharyya* [1999]

presented high-resolution *F* region plasma drift and backscatter echo intensity maps showing that a strong plasma shear flow (with eastward drift above and westward drift below a transition height near 300 km) existed in the postsunset equatorial *F* region bottomside. A BSL was found to be situated below the null point of the shear flow (in the westward flow region). They suggested that in this region, the large differential velocity between the plasma (westward) and neutrals (eastward) after sunset could drive an interchange instability process and thus cause the generation of BSL. Results from the Jicamarca radar observations and the TIEGCM simulations have shown that the plasma shear vortex structure occurs exclusively after sunset [e.g., *Kudeki and Bhattacharyya*, 1999; *Rodrigues et al*., 2012]. Specifically, in an experiment involving a combination of sounding rockets, the Altair radar and a collocated Digisonde conducted over Kwajalein, *Hysell et al*. [2005] found direct evidence that the postsunset bottom-type irregularities, which usually drift westward, were situated in the altitude region where the westward background plasma drifts were the strongest. These observations demonstrated that the generation of postsunset BSL is directly associated with the westward plasma drifts as part of the postsunset equatorial *F* region plasma flow vortex.

However, the occurrence of BSL at low latitudes far away from the magnetic equator and well before sunset (about 1 h earlier than the onset of the plasma flow vortex reported previously) is unlikely to be driven by the equatorial plasma shear flow. Over Sanya and Fuke, the altitudes of 200 km or higher where the presunset BSL were observed correspond to apex altitudes of more than 500 km over the magnetic equator. If the presunset BSL observed by the two radars were linked with the equatorial plasma shear flow (and its associated BSL), it would require the equatorial plasma shear vortex flow to be centered at a relatively high altitude (more than 500 km) and to occur well before sunset. In this regard, however, there is still no direct observation reported, to the best of our knowledge, to show that the equatorial plasma shear vortex emerges well before sunset.

In this context we may note in Figures 3c and 3d an additional feature of the presunset BSL in that the oscillation shown in the BSL echo Doppler velocities is very similar to the *F* layer height perturbation. Similar perturbations in *F* layer heights (as that shown in Figure 3d) have recently been reported on the basis of Digisonde measurements over Fortaleza [e.g., *Abdu et al*., 2009; *Takahashi et al*., 2010]. From a statistical analysis of about 2 month of Digisonde data, *Abdu et al*. [2015] found that the small-amplitude perturbations in the *F* layer heights with a period of 0.5–1.5 h (which corresponded to LSWS with wavelengths ranging from several hundreds to thousands of kilometers) appeared during presunset and continued their development until the occurrence of ESF plume. It was suggested that the height perturbations that could indicate the presence of wave structures in polarization electric field were induced by gravity wave wind perturbations.

For the gravity wave perturbation wind component ($\boldsymbol{U_g}$) normal to the magnetic field $\boldsymbol{B}$, to drive a current, a polarization electric field $\boldsymbol{E_p}$ (antiparallel to $\boldsymbol{U_g} \times \boldsymbol{B}$) must build up to keep the net current divergence zero. The zonal component of the $\boldsymbol{E_p}$ (that could be caused by vertical and meridional winds) might cause the Doppler velocity oscillation. An important point to note in this context concerns the sustenance of *F* region bottomside $\boldsymbol{E_p}$ during the presunset hours, in view of the possibility that the daytime *E* region conductivity, in general, may be large enough to cause the shorting of the $\boldsymbol{E_p}$. Through calculation of the ratio of the field line integrated Pedersen conductivities of ionospheric *E* and *F* regions, *Abdu et al*. [2015] showed in a recent investigation that the $\boldsymbol{E_p}$ can indeed be sustained during several hours preceding sunset. According to them, the off-equatorial *E* region might not completely short out the *F* region polarization electric field generated by gravity waves, and hence, the zonal $\boldsymbol{E_p}$ could cause oscillations of BSL Doppler velocity and of the *F* layer heights, through the $(\boldsymbol{E} \pm \text{zonal } \boldsymbol{E_p}) \times \boldsymbol{B}$ vertical drift (where $\boldsymbol{E}$ is the background eastward electric field).

As regard the mechanism responsible for the generation of low-latitude *F* region irregularity, there could be several possibilities including gradient drift instabilities driven by gravity (g/ν_{in}), wind (U), or electric field (E). For the $\boldsymbol{E} \times \boldsymbol{B}$-driven gradient drift instability, the zonal (vertical) electric field acting on the vertical (horizontal) density gradient might favor the irregularity growth. On the other hand, the wind, if achieving sufficient speed in the direction antiparallel to plasma density gradient, could directly drive gradient drift instability and generate irregularities. Based on the feature that bottom-type irregularities were horizontally aligned in thin layers without altitude extension, *Hysell et al*. [2004] concluded that the irregularity should be generated from the gradient drift instability driven by horizontal wind, instead of by electric field [see also *Linson and Workman*, 1970]. For the present study, the observed features of the altitude morphology (thin layer, not developing vertically) and spectral characteristics (narrow width) of the presunset BSL echoes are very similar to those of BSL echoes

observed around the magnetic equator after sunset. It is quite likely that the mechanism responsible for the presunset BSL could be similar to that of the postsunset BSL, i.e., the wind-driven gradient drift instability. For the instability development, a large enough horizontal wind (U) would be required to provide the driving force U-V, where V is the plasma zonal drift speed. However, considering the uncertain and small values ($<10\ \mathrm{m\ s^{-1}}$) of the background neutral and plasma zonal velocities at presunset hours [*Heelis et al*., 2012], it is unlikely that the background wind can drive the gradient drift instability. One important question for the present presunset BSL concerns the source of the U responsible for driving the gradient drift instability.

From the preliminary statistical results presented in the section 4, we can see that the presunset BSL events were often observed on the evenings when F layer height oscillations with downward phase propagation were present, indicating the presence of gravity waves propagating upward to the F region (as mentioned above). Using observational data from the SpreadFEx campaign, *Fritts et al*. [2008] suggested that the perturbation horizontal wind due to upward propagating gravity wave could reach up to $100\ \mathrm{m\ s^{-1}}$ in the F region bottomside. Such large perturbation westward/eastward winds, acting on strong eastward/westward density gradients, might cause the generation of BSL. For the wind-driven gradient drift instability, the linear growth rate γ is given by

$$\gamma = \frac{(U - V)}{L},$$

where the zonal wind U contains contributions from both the gravity wave perturbation winds and background zonal winds, V is the plasma zonal drift speed, and L is the scale length of plasma density gradient in the U-V direction. Assuming a value of (say) 15° for the layer tilt, the zonal component of the density gradient in the BSL is given by $L = L_V/\sin 15°$, where L_V is the vertical gradient scale length [see also *MacDougall et al*., 1998]. For positive value of U-V, which is antiparallel to the plasma density gradient, the growth rate is always positive. If we assume values of $100\ \mathrm{m\ s^{-1}}$ and 20 km for U-V and L_V, respectively, the e-folding time of the instability growth would be about 13 min, indicating the number of e-folds about 5 over 1 h. If U-V is not sufficiently strong, the growth of the instability may be slow and, depending upon the duration of the wind and the layer tilt, it may fail to produce the BSL.

It is relevant to mention that the values of U-V and L_V, assumed as $100\ \mathrm{m\ s^{-1}}$ and 20 km, respectively, in the above analysis, may not be the same as those for the cases of presunset BSL observations. Usually, stronger U-V is more favorable for the instability growth. But even if a strong driver (e.g., gravity wave perturbation wind) exists, a combination of its duration, the layer tilt, and density gradient may fail to produce the BSL. On the other hand, even when the driving wind is not sufficiently strong, a combination of the other factors may contribute to a slow or normal growth of the instability, and thus produce the BSL if the driver exists for a long enough time. For example, when the U-V is $50\ \mathrm{m\ s^{-1}}$, the e-folds of growth over 2 hs will be the same as that of the instability driven by the U-V of $100\ \mathrm{m\ s^{-1}}$ over 1 h. For the present data set, it is a challenging task to evaluate the minimum level of wind (U) and plasma drift speeds (V) required for the growth of instability producing presunset BSL. Direct measurements of U and V together with simultaneous observations of presunset BSL and of background ionosphere will be critical. This should be possible in future with the completion of the Sanya ISR which is under construction and with the realization of the sounding rocket experiments planned in the second phase of the Chinese Meridional Project.

6. Conclusions

We have presented simultaneous radar observations of a BSL generated before sunset extending until the appearance of ESF plume, over two low-latitude locations Sanya and Fuke. The altitude morphology and the extremely narrow spectral width of the BSL echoes resemble closely those reported for the postsunset equatorial ionosphere. However, the present BSL occurred well before sunset, much earlier than that reported previously. The presunset BSL echo Doppler velocity showed oscillations with a period of about 1 h, similar to the simultaneously observed oscillation in F layer height/density. The presunset characteristics of this event indicate that the source responsible for this type of BSL is different from that of the equatorial postsunset BSL. A preliminary statistics from the Sanya radar observations showed that the presunset BSLs were observed on the days with F layer height oscillations presenting downward phase propagation. The plasma instability-driven by gravity waves, instead of by the equatorial plasma shear vortex flow, is proposed to be the likely mechanism for the BSL generated before sunset. The results could build a link between the F layer density perturbations (large-scale wave structure) and the BSL both generated before sunset.

Acknowledgments

This research is supported by the National Natural Science Foundation of China (41422404, 41374163, and 41374164) and the Specialized Research Fund for State Key Laboratories, and the National High Technology Research and Development Program of China (863 Program, 2014AA123501). The Sanya and Fuke data can be obtained through ftp://159.226.119.167 and data.meridianproject.ac.cn (registration required) or on request from G.L. (gzlee@mail.iggcas.ac.cn) and C.Y. (cxyan@space-weather.ac.cn), respectively. M.A.A. acknowledges the support from CAPES for a senior visiting professorship at ITA. We acknowledge the use of Fuke radar data from the Chinese Meridian Project. The reviewers' comments that greatly improved the sections 4 and 5 are appreciated.

References

Abdu, M. A., E. A. Kherani, I. S. Batista, E. R. de Paula, D. C. Fritts, and J. H. A. Sobral (2009), Gravity wave initiation of equatorial spread F/plasma bubble irregularities based on observational data from the SpreadFEx campaign, *Ann. Geophys.*, *27*, 2607–2622, doi:10.5194/angeo-27-2607-2009.

Abdu, M. A., J. R. de Souza, E. A. Kherani, I. S. Batista, J. W. MacDougall, and J. H. A. Sobral (2015), Wave structure and polarization electric field development in the bottomside F layer leading to postsunset equatorial spread F, *J. Geophys. Res. Space Physics*, *120*, 6930–6940, doi:10.1002/2015JA021235.

Chen, G., H. Jin, X. Huang, D. Zhong, C. Yan, and G. Yang (2015), Strong correlation between quasi periodic echoes and plasma drift in the E region, *J. Geophys. Res. Space Physics*, *120*, 9110–9116, doi:10.1002/2015JA021566.

Fritts, D. C., et al. (2008), Gravity wave and tidal influences on equatorial spread F based on observations during the spread F experiment (SpreadFEx), *Ann. Geophys.*, *26*, 3235–3252, doi:10.5194/angeo-26-3235-2008.

Heelis, R. A., G. Crowley, F. Rodrigues, A. Reynolds, R. Wilder, I. Azeem, and A. Maute (2012), The role of zonal winds in the production of a pre-reversal enhancement in the vertical ion drift in the low latitude ionosphere, *J. Geophys. Res.*, *117*, A08308, doi:10.1029/2012JA017547.

Hysell, D. L., and J. D. Burcham (1998), JULIA radar studies of equatorial spread F, *J. Geophys. Res.*, *103*(A12), 29,155–29,167, doi:10.1029/98JA02655.

Hysell, D. L., J. Chun, and J. L. Chau (2004), Bottom-type scattering layers and equatorial spread F, *Ann. Geophys.*, *22*, 4061–4069, doi:10.5194/angeo-22-4061-2004.

Hysell, D. L., M. F. Larsen, C. M. Swenson, A. Barjatya, T. F. Wheeler, M. F. Sarango, R. F. Woodman, and J. L. Chau (2005), Onset conditions for equatorial spread F determined during EQUIS II, *Geophys. Res. Lett.*, *32*, L24104, doi:10.1029/2005GL024743.

Hysell, D. L., M. F. Larsen, C. M. Swenson, A. Barjatya, T. F. Wheeler, T. W. Bullett, M. F. Sarango, R. F. Woodman, J. L. Chau, and D. Sponseller (2006), Rocket and radar investigation of background electrodynamics and bottom-type scattering layers at the onset of equatorial spread F, *Ann. Geophys.*, *24*, 1387–1400, doi:10.5194/angeo-24-1387-2006.

Kudeki, E., and S. Bhattacharyya (1999), Post-sunset vortex in equatorial F-region plasma drifts and implications for bottomside spread-F, *J. Geophys. Res.*, *104*, 28,163–28,170, doi:10.1029/1998JA900111.

Li, G., B. Ning, M. A. Abdu, W. Wan, and L. Hu (2012), Precursor signatures and evolution of post-sunset equatorial spread-F observed over Sanya, *J. Geophys. Res.*, *117*, A08321, doi:10.1029/2012JA017820.

Li, G., B. Ning, M. A. Abdu, Y. Otsuka, T. Yokoyama, M. Yamamoto, and L. Liu (2013), Longitudinal characteristics of spread F backscatter plumes observed with the EAR and Sanya VHF radar in Southeast Asia, *J. Geophys. Res. Space Physics*, *118*, 6544–6557, doi:10.1002/jgra.50581.

Li, G., Y. Otsuka, B. Ning, M. A. Abdu, M. Yamamoto, W. Wan, L. Liu, and P. Abadi (2016), Enhanced ionospheric plasma bubble generation in more active ITCZ, *Geophys. Res. Lett.*, *43*, 2389–2395, doi:10.1002/2016GL068145.

Linson, L. M., and J. B. Workman (1970), Formation of striation in ionospheric plasma clouds, *J. Geophys. Res.*, *75*, 3211–3219, doi:10.1029/JA075i016p03211.

MacDougall, J. W., M. A. Abdu, P. T. Jayachandran, J.-F. Cecile, and I. S. Batista (1998), Pre sunrise spread F over Fortaleza, *J. Geophys. Res.*, *103*(A10), 23,413–23,425, doi:10.1029/98JA01949.

Patra, A. K., P. Srinivasulu, P. P. Chaitanya, M. D. Rao, and A. Jayaraman (2014), First results on low-latitude E and F region irregularities obtained using the Gadanki Ionospheric Radar Interferometer, *J. Geophys. Res. Space Physics*, *119*, 10,276–10,293, doi:10.1002/2014JA020604.

Rodrigues, F. S., E. R. de Paula, M. A. Abdu, A. C. Jardim, K. N. Iyer, P. M. Kintner, and D. L. Hysell (2004), Equatorial spread F irregularity characteristics over Sao Luis, Brazil, using VHF radar and GPS scintillation techniques, *Radio Sci.*, *39*, RS1S31, doi:10.1029/2002RS002826.

Rodrigues, F. S., G. Crowley, R. A. Heelis, A. Maute, and A. Reynolds (2012), On TIE-GCM simulation of the evening equatorial plasma vortex, *J. Geophys. Res.*, *117*, A05307, doi:10.1029/2011JA017369.

Takahashi, H., et al. (2010), Equatorial ionosphere bottom-type spread F observed by OI 630.0 nm airglow imaging, *Geophys. Res. Lett.*, *37*, L03102, doi:10.1029/2009GL041802.

Tsunoda, R. T., and W. L. Ecklund (2007a), On the post-sunset rise of the equatorial F layer and superposed upwellings and bubbles, *Geophys. Res. Lett.*, *34*, L04101, doi:10.1029/2006GL028832.

Tsunoda, R. T., and W. L. Ecklund (2007b), On the visibility and zenithal confinement of 150 km (F1) radar echoes, *Geophys. Res. Lett.*, *34*, L21102, doi:10.1029/2007GL031276.

Tsunoda, R. T., D. M. Bubenik, S. V. Thampi, and M. Yamamoto (2010), On large-scale wave structure and equatorial spread F without a postsunset rise of the F layer, *Geophys. Res. Lett.*, *37*, L07105, doi:10.1029/2009GL042357.

Wang, C. (2010), New chains of space weather monitoring stations in China, *Space Weather*, *8*, S08001, doi:10.1029/2010SW000603.

Woodman, R. F., and C. La Hoz (1976), Radar observations of F region equatorial irregularities, *J. Geophys. Res.*, *81*, 5447–5466, doi:10.1029/JA081i031p05447.